

Lyapunov-Based Control for Flat-Spin Recovery and Spin Inversion of Spin-Stabilized Spacecraft

Zachary R. Manchester*
Harvard University, Cambridge, Massachusetts, 02138

Lyapunov-based control laws capable of performing flat-spin recovery and spin-inversion maneuvers for spin-stabilized spacecraft with reaction wheels are presented. The advantages of the Lyapunov-based control laws over previous approaches include the ability to explicitly account for actuator limits and a proof of almost-global asymptotic stability. Numerical examples are presented to illustrate the performance of the controllers.

Nomenclature

h	=	angular momentum in body-fixed axes
I	=	inertia tensor in body-fixed axes
$\mathbf{I}_{n \times n}$	=	$n \times n$ identity matrix
J	=	inverse inertia tensor in body-fixed axes
k	=	discrete time index
t	=	time
T	=	nutation period
u	=	matrix of sampled control inputs
V	=	Lyapunov function
x	=	matrix of sampled states
δ_t	=	time step
ρ	=	rotor angular momentum in body-fixed axes
ω	=	angular velocity in body-fixed axes

I. Introduction

Flat-spin recovery is a classic problem in spacecraft dynamics and control with a rich history dating back to the very first man-made satellites [1]. Fundamentally, the problem has its roots in the geometry of rockets and the fairings that house satellites during launch, which tend to be long and narrow. As a result, most spacecraft have prolate mass distributions, at least in their launch configurations.

In the presence of energy dissipation due, for example, to fluid slosh or flexible structural elements, a spacecraft spinning about its long axis, or minor axis of inertia, will tend to transition into a spin about its major axis, commonly known as a flat spin. Maintaining a minor-axis spin, therefore, requires active control. While spin-stabilized satellites have largely been supplanted by three-axis stabilized designs, many missions still call for spacecraft to spin about their minor axes temporarily, especially during critical phases like deployments and orbit insertion maneuvers [2]. Additionally, low-cost small satellites are frequently designed as minor-axis spinners, both to provide stabilization and to meet other mission requirements [3–5].

Many authors have analyzed variations of the flat-spin recovery problem over the past several decades. In its most basic form, the problem entails controlling a spacecraft in such a way that it transitions from a major-axis spin to a minor-axis spin. Early methods focused on utilizing thrusters as actuators [2, 6], however these have the disadvantage of consuming limited propellant resources. In the 1970s, Gebman and Mingori used perturbation methods to analyze control techniques for flat-spin recovery of dual-spin spacecraft in which actuation is provided by a motor applying internal torques parallel to the desired spin axis [7]. While these methods do not consume fuel, they have the disadvantage of leaving the spacecraft with residual nutation that must be damped out by some other means.

More recently, Lawrence and Holden have developed Lyapunov-based control laws for a spacecraft with a single reaction wheel mounted transverse to the desired spin axis [8]. While their method offers some asymptotic stability guarantees, their controller suffers from one potentially major drawback: It cannot determine the sign of the final body-frame angular momentum vector. Depending on initial conditions, the spacecraft could find itself rotated 180° from the desired orientation.

The problem of effecting a 180° inversion of a spacecraft's spin axis has often been treated separately from flat-spin recovery. Rahn and Barba have proposed a method for "spin polarity control" using thrusters [9]. Beachey and Uicker describe a method for inverting the spin of an axisymmetric spinning spacecraft using a single reaction wheel [10].

*Postdoctoral Fellow, School of Engineering and Applied Sciences, 60 Oxford Street, Member, zmanchester@seas.harvard.edu

Uicker has also proposed a method for inverting a spacecraft’s spin axis by manipulating its mass distribution [11].

To the author’s best knowledge, the first unified treatment of flat-spin recovery and spin inversion, in the form of a single controller capable of uniquely determining a spacecraft’s final spin axis, was given by Myung and Bang [12]. They make use of a control technique known as predictive control [13] to derive a nonlinear feedback law for a spacecraft with a single reaction wheel. While they demonstrate numerically that their controller converges to the desired spin axis in many cases, they do not give strong stability guarantees. Additionally, their controller does not explicitly account for actuator limits and must be carefully tuned based on system parameters.

In this paper, a family of nonlinear feedback control laws capable of driving a spinning spacecraft from any initial state to a desired minor-axis spin using reaction wheels is developed. The controllers provide almost-global asymptotic stability and can explicitly accommodate actuator limits. Additionally, the feedback laws have a simple and explicit mathematical form and are easy to tune and implement.

The paper proceeds as follows: Section II provides a review of relevant spacecraft dynamics as well as Lyapunov stability theory. Next, sections III and IV introduce and analyze several candidate Lyapunov functions. Section V analyzes the global stability properties of controllers based on a particular choice of Lyapunov function. Section VI then discusses the implementation of a family of control laws which are almost-globally asymptotically stabilizing. The control laws are then demonstrated in numerical examples in section VIII. Finally, conclusions are outlined in section IX.

II. Background

This section provides brief reviews of gyrostat dynamics and Lyapunov stability. It also serves to introduce the notation and terminology used throughout the rest of the paper. Thorough treatments of Lyapunov stability are given by Khalil [14] and Slotine and Li [15], while a thorough treatment of gyrostat dynamics is given by Hughes [16].

A. Gyrostat Dynamics

A gyrostat is a system of coupled rigid bodies whose relative motions do not change the total inertia tensor of the system. This abstraction serves as a practical mathematical model for a spacecraft with reaction wheels. The fundamental differential equation governing the motion of a gyrostat is [16],

$$I \cdot \dot{\omega} + \omega \times (I \cdot \omega + \rho) + \dot{\rho} = \tau \quad (1)$$

where I is the symmetric positive-definite inertia tensor of the gyrostat, ω is the body angular velocity, ρ is the total angular momentum stored in the rotors, and τ is the external torque applied to the gyrostat. Assuming external torques can be neglected, the total system angular momentum,

$$\mathbf{h} = I \cdot \omega + \rho \quad (2)$$

is conserved, and the gyrostat equation can be rewritten as,

$$\dot{\mathbf{h}} = \mathbf{h} \times J \cdot (\mathbf{h} - \rho) \quad (3)$$

where $J = I^{-1}$.

The dynamics of equation (3) have some properties that will be useful in the controller development to follow. First, because $\|\mathbf{h}\|$ is conserved, \mathbf{h} is confined to the surface of a sphere, which will be referred to as the *momentum sphere*. Second, for a fixed value of ρ , the solutions to equation (3) are periodic. In fact, $\mathbf{h}(t)$ can be expressed in closed form in terms of Jacobi elliptic functions [17, 18]. The details of these solutions will not be of concern in this paper, only their existence and periodicity. Lastly, in the case where $\rho = 0$, the uncontrolled system has, in general, six equilibria located along the eigenvectors of J . The equilibrium points corresponding to the largest and smallest eigenvalues of J (commonly referred to as the “minor” and “major” axes, respectively) are stable, while those corresponding to the intermediate eigenvalue are unstable [16].

Figure 1 depicts a momentum sphere with several trajectories marked in blue and the equilibria marked in green. Each of the four stable equilibria are surrounded by stable periodic orbits. The trajectories marked in red in figure 1 are known as *separatrices* [16]. They connect the two unstable equilibria and separate trajectories orbiting the other four equilibria.

B. Lyapunov Stability

Lyapunov stability theory provides a means for determining the stability of equilibrium points of nonlinear dynamical systems. The method provides a generalization of the concept of energy dissipation in damped mechanical systems.

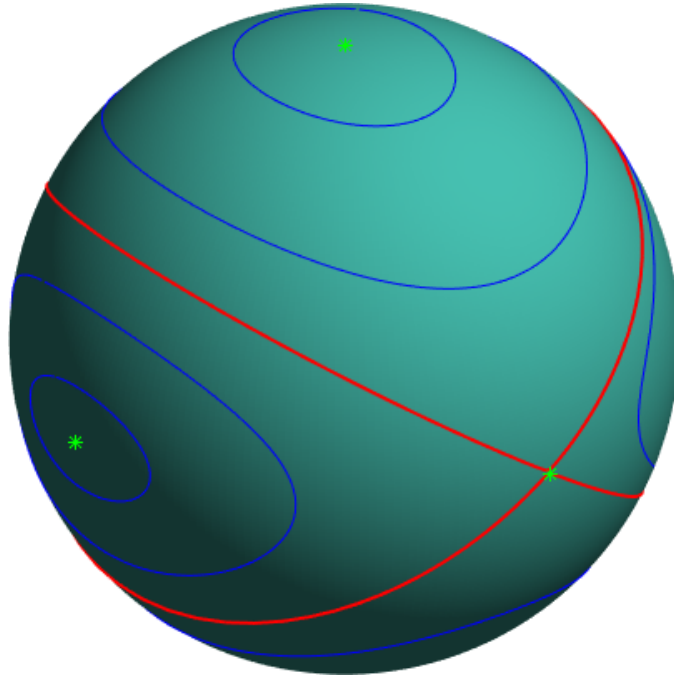


Figure 1. Momentum sphere with equilibria and example trajectories

The necessary ingredients are a system of the form,

$$\dot{x} = f(x) \quad (4)$$

where $x \in \mathbb{R}^n$, an equilibrium point x^* such that,

$$f(x^*) = 0 \quad (5)$$

and a scalar function $V(x)$ with the property,

$$V(x) \geq 0 \quad (6)$$

where $V(x) = 0$ only at the point $x = x^*$. If the derivative of $V(x)$ along trajectories of the system,

$$\dot{V}(x) = \frac{\partial V}{\partial x} \frac{dx}{dt} = \nabla V(x) \cdot f(x) \quad (7)$$

is negative-semidefinite, the system is said to be stable *in the sense of Lyapunov*. If the stricter condition $\dot{V}(x) < 0$ everywhere except at $x = x^*$, the system is *asymptotically stable*. The main deficiency of Lyapunov stability theory is that there are no general methods for finding or constructing a function $V(x)$, which is known as a Lyapunov function.

For a dynamical system with control inputs,

$$\dot{x} = f(x, u) \quad (8)$$

where $x \in \mathbb{R}^n$ and $u \in \mathbb{R}^m$, a Lyapunov function can be used to find stabilizing control laws. In the controlled case, the stability condition becomes:

$$\dot{V}(x, u) = \nabla V(x) \cdot f(x, u) \leq 0 \quad (9)$$

A controller can then be found by, for example, solving the following optimization problem,

$$\begin{aligned} \underset{u}{\operatorname{argmin}} \quad & \nabla V(x) \cdot f(x, u) \\ \text{subject to} \quad & u \in \mathcal{U} \end{aligned} \quad (10)$$

where \mathcal{U} is the set of possible control inputs. If u can be chosen such that $\dot{V}(x, u) < 0$ for every $x \neq x^*$, the closed loop system will be asymptotically stable.

III. Candidate Lyapunov Functions

As motivation, two candidate Lyapunov functions are considered. The first is a quadratic function based on kinetic energy,

$$V_Q = \frac{1}{2} \mathbf{h}_d \cdot \mathbf{J} \cdot \mathbf{h}_d - \frac{1}{2} \mathbf{h} \cdot \mathbf{J} \cdot \mathbf{h} \quad (11)$$

while the second is a linear function,

$$V_L = \mathbf{h}_d \cdot \mathbf{J} \cdot \mathbf{h}_d - \mathbf{h}_d \cdot \mathbf{J} \cdot \mathbf{h} \quad (12)$$

where \mathbf{h}_d is the desired minor-axis equilibrium angular momentum vector. Since \mathbf{h}_d corresponds to a spin state with maximum kinetic energy, it is easy to show that both V_Q and V_L are non-negative everywhere on the momentum sphere, satisfying condition (6).

Looking first at V_Q and taking its derivative along trajectories of the system yields:

$$\dot{V}_Q = \frac{\partial V_Q}{\partial \mathbf{h}} \frac{d\mathbf{h}}{dt} = \mathbf{h} \cdot \mathbf{J} \cdot \mathbf{h} \times \mathbf{J} \cdot \boldsymbol{\rho} \quad (13)$$

As expected, when $\boldsymbol{\rho} = 0$, V_Q does not vary. With an appropriate choice of $\boldsymbol{\rho}$, the condition $\dot{V}_Q \leq 0$ can always be satisfied, indicating that the closed loop system will be stable. It must be noted, however, that V_Q is symmetric and possesses a pair of global minima located at $\mathbf{h} = \mathbf{h}_d$ and $\mathbf{h} = -\mathbf{h}_d$. As a result, the system can only be guaranteed to converge to one or the other of these equilibrium states, with the result depending on initial conditions. Figure 2 depicts a heat map of the function V_Q on the momentum sphere, with \mathbf{h}_d marked in green.

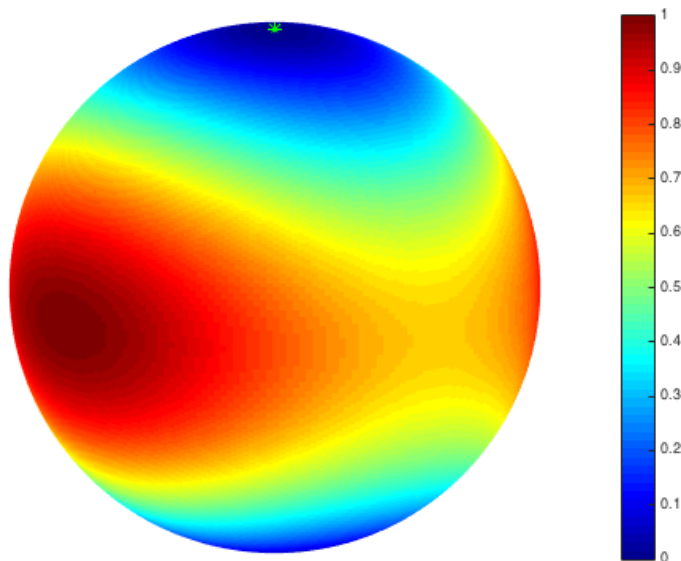


Figure 2. Heat map of candidate Lyapunov function V_Q

Unlike V_Q , V_L has the advantage of possessing a single global minimum on the momentum sphere at $\mathbf{h} = \mathbf{h}_d$, as can be seen in figure 3. Therefore, if a control law can be found which drives V_L to zero, the system is guaranteed to converge to \mathbf{h}_d . Unfortunately, V_L also suffers from several disadvantages. Evaluating its derivative with respect to time results in:

$$\dot{V}_L = \frac{\partial V_L}{\partial \mathbf{h}} \frac{d\mathbf{h}}{dt} = -\mathbf{h}_d \cdot \mathbf{J} \cdot \mathbf{h} \times \mathbf{J} \cdot (\mathbf{h} - \boldsymbol{\rho}) \quad (14)$$

Note that, unlike what was encountered with V_Q , when $\boldsymbol{\rho} = 0$, $\dot{V}_L \neq 0$, meaning that V_L varies along uncontrolled system trajectories. In the presence of actuator limits, where the maximum-possible rotor momentum $\|\boldsymbol{\rho}\|$ might be much smaller than $\|\mathbf{h}\|$, there may be situations in which the condition $\dot{V}_L \leq 0$ cannot be satisfied.

IV. Periodic Averaging

A variation on equation (12) will now be considered that mitigates some of the problems encountered in the previous section. A new candidate Lyapunov function V'_L is obtained by averaging V_L over periodic orbits of the uncontrolled

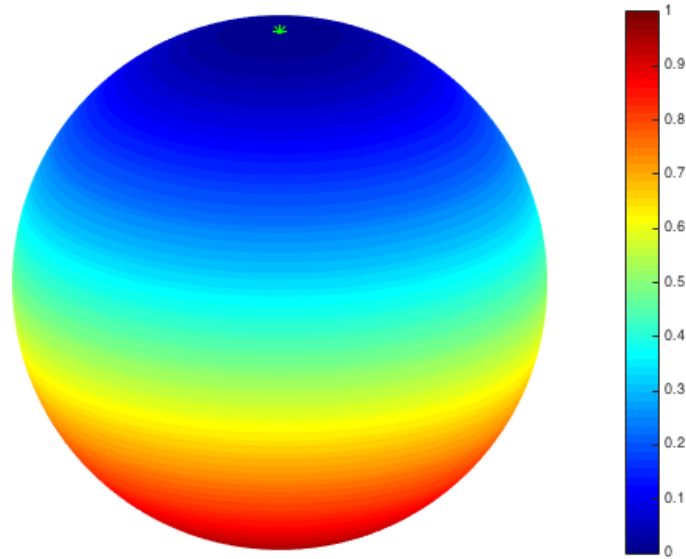


Figure 3. Heat map of candidate Lyapunov function V_L

system, where T is the nutation period:

$$V'_L = \mathbf{h}_d \cdot \mathbf{J} \cdot \mathbf{h}_d - \frac{1}{T} \int_{t_0}^{t_0+T} \mathbf{h}_d \cdot \mathbf{J} \cdot \mathbf{h}(t) dt \quad (15)$$

It is worth noting that V'_L is a function only of the current state \mathbf{h} . While it does not have a convenient closed-form expression like V_L or V_Q , it could be, for example, precomputed over the entire momentum sphere and tabulated in a look-up table.

By construction, V'_L takes on the same value at every point along a given periodic orbit. Therefore, it does not vary along trajectories of the uncontrolled system. Also, like V_L , V'_L has a single global minimum at $\mathbf{h} = \mathbf{h}_d$, as shown in figure 4. Unfortunately, V'_L still suffers from one important deficiency: As can be understood based on

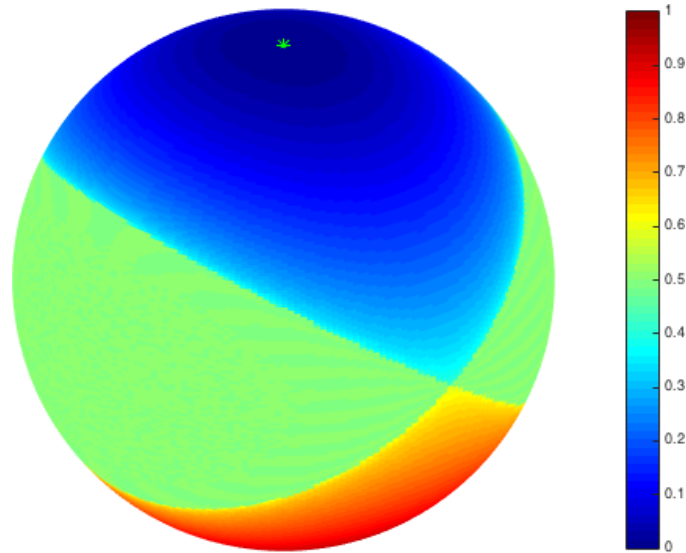


Figure 4. Heat map of candidate Lyapunov function V'_L

simple symmetry considerations and seen in figure 4, V'_L is constant over the entirety of the regions surrounding the major-axis equilibria. As a result, $\dot{V}'_L = 0$, and the system will not converge to \mathbf{h}_d from initial conditions in those regions.

A Lyapunov function will now be formed from the sum of V_Q and V'_L , combining the behavior of the former in regions near the major-axis equilibria with the behavior of the latter in regions near the minor-axis equilibria:

$$V = \frac{3}{2} \mathbf{h}_d \cdot \mathbf{J} \cdot \mathbf{h}_d - \frac{1}{T} \int_{t_0}^{t_0+T} \mathbf{h}_d \cdot \mathbf{J} \cdot \mathbf{h}(t) + \frac{1}{2} \mathbf{h}(t) \cdot \mathbf{J} \cdot \mathbf{h}(t) dt \quad (16)$$

As with equation (15), the integral in equation (16) is taken over periodic orbits of the uncontrolled system. Figure 5 shows a heat map of V on the momentum sphere with \mathbf{h}_d marked in green.

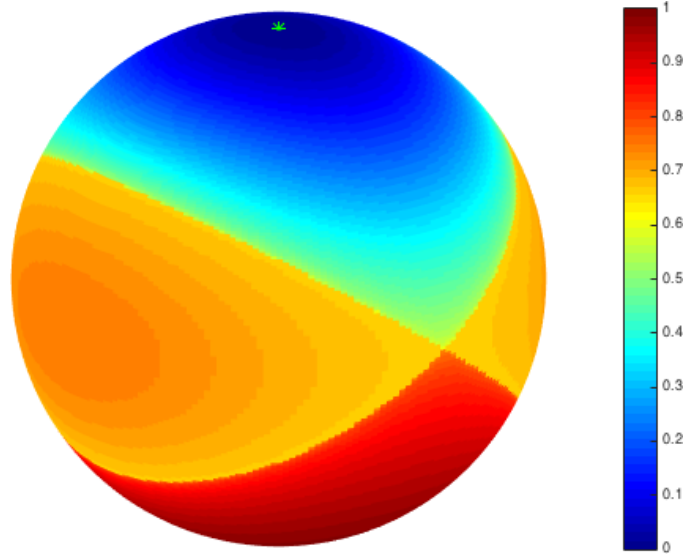


Figure 5. Heat map of Lyapunov function V

An expression for \dot{V} will now be sought. To aid in this process, the integral in equation (16) will be discretized. First, sampled versions of \mathbf{h} and $\boldsymbol{\rho}$ are defined,

$$\mathbf{h}_k = \mathbf{h}(t_0 + k\delta_t) \quad (17)$$

$$\boldsymbol{\rho}_k = \boldsymbol{\rho}(t_0 + k\delta_t) \quad (18)$$

where $\delta_t = T/N$ and N is the number of samples. Next, the following matrices, which consist of uniform samples of the state and control inputs, are defined:

$$x_k = \begin{bmatrix} \mathbf{h}_k \\ \vdots \\ \mathbf{h}_{k+N-1} \end{bmatrix} \quad u_k = \begin{bmatrix} \boldsymbol{\rho}_k \\ \vdots \\ \boldsymbol{\rho}_{k+N-1} \end{bmatrix} \quad (19)$$

In terms of x_k and u_k , the integral in equation (16) can be approximated as,

$$\int_{t_0}^{t_0+T} \mathbf{h}_d \cdot \mathbf{J} \cdot \mathbf{h} + \frac{1}{2} \mathbf{h} \cdot \mathbf{J} \cdot \mathbf{h} dt \approx \frac{1}{N} x_d^T \bar{\mathbf{J}} x_k + \frac{1}{2N} x_k^T \bar{\mathbf{J}} x_k \quad (20)$$

where x_d is,

$$x_d = \begin{bmatrix} \mathbf{h}_d \\ \vdots \\ \mathbf{h}_d \end{bmatrix} \quad (21)$$

and $\bar{\mathbf{J}}$ is the following block-diagonal matrix:

$$\bar{\mathbf{J}} = \begin{bmatrix} \mathbf{J} & 0 & \cdots & 0 \\ 0 & \mathbf{J} & \cdots & 0 \\ \vdots & \vdots & \ddots & \vdots \\ 0 & 0 & \cdots & \mathbf{J} \end{bmatrix} \quad (22)$$

The next step in determining \dot{V} is to calculate the following finite difference:

$$\Delta V = V(x_{k+1}) - V(x_k) = \frac{1}{N} x_d^\top \bar{J} x_k + \frac{1}{2N} x_k^\top \bar{J} x_k - \frac{1}{N} x_d^\top \bar{J} x_{k+1} - \frac{1}{2N} x_{k+1}^\top \bar{J} x_{k+1} \quad (23)$$

Thanks to periodicity, the system dynamics along an orbit can be approximated as,

$$x_{k+1} = Ax_k + B_k u_k \quad (24)$$

where A is a cyclic permutation matrix,

$$A = \begin{bmatrix} 0 & \mathbf{1}_{3 \times 3} & 0 & \cdots & 0 \\ 0 & 0 & \mathbf{1}_{3 \times 3} & \vdots & 0 \\ \vdots & \vdots & \ddots & \ddots & \vdots \\ 0 & 0 & \cdots & 0 & \mathbf{1}_{3 \times 3} \\ \mathbf{1}_{3 \times 3} & 0 & \cdots & 0 & 0 \end{bmatrix} \quad (25)$$

and B_k is the following block-diagonal matrix.

$$B_k = -\delta_t \begin{bmatrix} h_k^\times J & 0 & \cdots & 0 \\ 0 & h_{k+1}^\times J & 0 & \vdots \\ \vdots & \ddots & \ddots & 0 \\ 0 & \cdots & 0 & h_{k+N-1}^\times J \end{bmatrix} \quad (26)$$

The expression h^\times used in equation (26) denotes the formation of a 3×3 skew-symmetric cross-product matrix from the elements of h :

$$h^\times = \begin{bmatrix} 0 & -h_3 & h_2 \\ h_3 & 0 & -h_1 \\ -h_2 & h_1 & 0 \end{bmatrix} \quad (27)$$

Substituting equation (24) into equation (23) yields the following expression for ΔV :

$$\begin{aligned} \Delta V = & \frac{1}{N} x_d^\top \bar{J} x_k - \frac{1}{N} x_d^\top \bar{J} A x_k - \frac{1}{N} x_d^\top \bar{J} B_k u_k \\ & + \frac{1}{2N} x_k^\top \bar{J} x_k - \frac{1}{2N} x_k^\top A^\top \bar{J} A x_k - \frac{1}{N} x_k^\top A^\top \bar{J} B_k u_k - \frac{1}{2N} u_k^\top B_k^\top \bar{J} B_k u_k \end{aligned} \quad (28)$$

Because A is simply a permutation matrix, several terms in equation (28) cancel each other, resulting in:

$$\Delta V = -\frac{1}{N} x_d^\top \bar{J} B_k u_k - \frac{1}{N} x_k^\top A^\top \bar{J} B_k u_k - \frac{1}{2N} u_k^\top B_k^\top \bar{J} B_k u_k \quad (29)$$

Finally, \dot{V} is recovered by taking a limit:

$$\dot{V} = \lim_{N \rightarrow \infty} \frac{\Delta V}{\delta_t} = \frac{1}{T} \int_{t_0}^{t_0+T} (\mathbf{h} + \mathbf{h}_d) \cdot \mathbf{J} \cdot \mathbf{h} \times \mathbf{J} \cdot \boldsymbol{\rho} \, dt \quad (30)$$

V. Almost-Global Asymptotic Stability

The expression inside the integral in equation (30) is linear in the rotor momentum $\boldsymbol{\rho}$. To make this more explicit, the following vector is defined,

$$\mathbf{b}(\mathbf{h}) = -\mathbf{J} \cdot \mathbf{h} \times \mathbf{J} \cdot (\mathbf{h} + \mathbf{h}_d) \quad (31)$$

such that:

$$\mathbf{b} \cdot \boldsymbol{\rho} = (\mathbf{h} + \mathbf{h}_d) \cdot \mathbf{J} \cdot \mathbf{h} \times \mathbf{J} \cdot \boldsymbol{\rho} \quad (32)$$

In terms of \mathbf{b} , the problem of choosing a control input such that $\dot{V} \leq 0$ reduces to choosing $\boldsymbol{\rho}$ such that $\mathbf{b} \cdot \boldsymbol{\rho} \leq 0$.

Looking again at equation (30), it is clear that the condition for asymptotic stability, $\dot{V} < 0$, can be met as long as $\mathbf{b} \cdot \boldsymbol{\rho} < 0$ can be achieved at some point along every periodic orbit of the uncontrolled system. For the fully actuated case where the spacecraft has at least three reaction wheels, this is possible everywhere on the momentum sphere except at the single point $\mathbf{h} = -\mathbf{h}_d$, which is simultaneously an equilibrium point of the system and a point at which $\mathbf{b} = 0$. This failure is to be expected as, in general, constant (time-invariant) feedback laws cannot achieve global asymptotic stability for systems with rotational degrees of freedom [19]. In practice, however, this does not present a problem. Since $-\mathbf{h}_d$ is an unstable equilibrium of the closed-loop system, perturbations will ensure that the system does not remain there.

VI. Controller Implementation

If sufficient reaction wheel torque is available, wheel dynamics can effectively be ignored and direct control over ρ can be assumed. In this case, equation (31) can be applied directly to derive very simple controllers. For example, one possible feedback law is,

$$\rho = -kb \quad (33)$$

where k is a scalar gain.

The optimal choice of ρ , in the sense of decreasing V the fastest, can be found by minimizing $\mathbf{b} \cdot \rho$, as in equation (10). In the particular case of a spacecraft with three reaction wheels, each aligned with an axis of the body coordinate frame, such a control law assumes the following form in body coordinates,

$$\rho = -\rho_{\max} \text{sign}(b) \quad (34)$$

where ρ_{\max} is the maximum wheel momentum and $\text{sign}(b)$ denotes the element-wise signum function:

$$\text{sign}(x) = \begin{cases} 1 & : x > 0 \\ 0 & : x = 0 \\ -1 & : x < 0 \end{cases} \quad (35)$$

In cases where reaction wheel torque is limited and the assumption of direct control over ρ cannot be made, a control law that specifies $\dot{\rho}$ and respects torque limits is needed. One such controller can be derived by first defining a smoothed version of the controller (34), where the signum function is replaced with a hyperbolic tangent:

$$\rho = -\rho_{\max} \tanh(\alpha b) \quad (36)$$

The scalar parameter α in equation (36) can be tuned to set the maximum commanded torque $\dot{\rho}_{\max}$. Equation (36) is then differentiated with respect to time, which yields,

$$\dot{\rho} = \frac{\partial \rho}{\partial b} \frac{\partial b}{\partial h} \frac{dh}{dt} = -\rho_{\max} \alpha \text{diag}(\text{sech}^2(\alpha b)) J [(J(h + h_d))^\times - h^\times J] h^\times J (h - \rho) \quad (37)$$

where $\text{diag}(x)$ indicates the formation of a diagonal matrix from the elements of x :

$$\text{diag} \left(\begin{bmatrix} x_1 \\ x_2 \\ x_3 \end{bmatrix} \right) = \begin{bmatrix} x_1 & 0 & 0 \\ 0 & x_2 & 0 \\ 0 & 0 & x_3 \end{bmatrix} \quad (38)$$

While equation (37) can, in principle, provide explicit wheel torque commands, the stability results of the previous section are specified as conditions on the wheel momenta. Therefore, to ensure stability, an actual implementation should track the wheel momenta specified by equation (36) using, for example, PID motor controllers on each wheel.

VII. Disturbance Torques

According to the analysis of section V, stability of the closed-loop system does not depend on the momentum storage or torque capabilities of the reaction wheels. In theory, the system should converge to \mathbf{h}_d for even very small values of ρ_{\max} and $\dot{\rho}_{\max}$, though it may take a long time. In practice, however, disturbance torques due to both internal dynamics (e.g. fluid slosh and flexible structural modes) and external forces (e.g. atmospheric drag and solar pressure) can prevent convergence or cause the system to become unstable. This section develops some conditions on actuator performance under which convergence can be guaranteed, given bounds on the disturbance torque.

Returning to the equation of motion for the gyrostat, a disturbance term \mathbf{d} is added to equation (3):

$$\dot{\mathbf{h}} = \mathbf{h} \times J \cdot (\mathbf{h} - \rho) + \mathbf{d} \quad (39)$$

No particular form is assumed for the disturbance, only that an upper bound can be placed on its magnitude. Repeating the analysis of section IV, the derivative of the Lyapunov function \dot{V} is sought. Equation (24) now reads,

$$x_{k+1} = Ax_k + B_k u_k + d_k \quad (40)$$

where d_k is defined in the same way as x_k and u_k in equation (19), and consists of uniform samples of the disturbance input:

$$d_k = \delta_t \begin{bmatrix} d(t_0 + k\delta_t) \\ \vdots \\ d(t_0 + (k + N - 1)\delta_t) \end{bmatrix} \quad (41)$$

Substituting equation (40) into equation (23) reveals a new form of equation (29) with some additional terms:

$$\Delta V = -\frac{1}{N} x_d^\top \bar{J} B_k u_k - \frac{1}{N} x_k^\top A^\top \bar{J} B_k u_k - \frac{1}{2N} u_k^\top B_k^\top \bar{J} B_k u_k - \frac{1}{N} x_d^\top \bar{J} d_k - \frac{1}{N} x_k^\top A^\top \bar{J} d_k - \frac{1}{N} u_k^\top B_k^\top \bar{J} d_k - \frac{1}{2N} d_k^\top \bar{J} d_k \quad (42)$$

Taking a limit of equation (42) yields an expression for \dot{V} that includes disturbance torques:

$$\dot{V} = \lim_{N \rightarrow \infty} \frac{\Delta V}{\delta t} = \frac{1}{T} \int_{t_0}^{t_0+T} (\mathbf{h} + \mathbf{h}_d) \cdot \mathbf{J} \cdot \mathbf{h} \times \mathbf{J} \cdot \boldsymbol{\rho} - (\mathbf{h} + \mathbf{h}_d) \cdot \mathbf{J} \cdot \mathbf{d} dt \quad (43)$$

The Lyapunov stability condition $\dot{V} \leq 0$ then becomes:

$$(\mathbf{h} + \mathbf{h}_d) \cdot \mathbf{J} \cdot \mathbf{h} \times \mathbf{J} \cdot \boldsymbol{\rho} \leq (\mathbf{h} + \mathbf{h}_d) \cdot \mathbf{J} \cdot \mathbf{d} \quad (44)$$

Given an upper bound d_{\max} on the magnitude of \mathbf{d} , equation (44) becomes:

$$(\mathbf{h} + \mathbf{h}_d) \cdot \mathbf{J} \cdot \mathbf{h} \times \mathbf{J} \cdot \boldsymbol{\rho} \leq -d_{\max} \|\mathbf{J} \cdot (\mathbf{h} + \mathbf{h}_d)\| \quad (45)$$

When sizing actuators in an engineering application, they should be chosen such that their maximum momentum storage capability ρ_{\max} allows the condition of (45) to be met given all anticipated values \mathbf{h} , \mathbf{h}_d , and \mathbf{J} .

VIII. Examples

This section presents two simulations that illustrate the performance of the control laws developed in section VI in the presence of model uncertainty and actuator limits. Both simulations are performed using MATLAB's ODE45 variable-step Runge-Kutta solver [20] with default error tolerances. To demonstrate the robustness of the controllers, the following nominal inertia is used in the controller,

$$I = \begin{bmatrix} 2 & 0 & 0 \\ 0 & 1.5 & 0 \\ 0 & 0 & 1 \end{bmatrix} \quad (46)$$

while the true inertia used to simulate the dynamics differs by 5% in the the moments of inertia and 5° in the orientation of the principal axes:

$$I_{\text{true}} = \begin{bmatrix} 2.0961 & -0.0455 & 0.0299 \\ -0.0455 & 1.4271 & 0.0167 \\ 0.0299 & 0.0167 & 1.0517 \end{bmatrix} \quad (47)$$

Additionally, white noise is added to the simulated gyro measurements fed to the controller.

The first simulation illustrates the performance of the controller (36) in a flat-spin recovery maneuver on a spacecraft with three reaction wheels. The initial angular momentum is,

$$h_0 = \begin{bmatrix} 1 \\ 0 \\ 0 \end{bmatrix} \quad (48)$$

and the desired final angular momentum is set to,

$$h_d = \begin{bmatrix} 0 \\ 0 \\ 1 \end{bmatrix} \quad (49)$$

which corresponds to an angular velocity of roughly 10 RPM about the minor axis. The maximum reaction wheel momentum is $\rho_{\max} = 0.01$ N·m·s, and the maximum reaction wheel torque is $\dot{\rho}_{\max} = 0.1$ N·m. The parameter α is set to a value of 60, which ensures that commanded torques are within the actuator saturation limits.

Figure 6 shows the closed-loop trajectory of the system, while figures 7–9 show the system momentum, reaction wheel momentum, and reaction wheel torque components, respectively. Rapid convergence to the desired minor axis-spin is achieved. The residual error in the angular momentum components and non-zero steady-state reaction wheel momenta are due to the error in the inertia used in the controller.

The second test case uses the same system and controller parameters but a different initial condition to illustrate the control law's ability to perform spin inversion maneuvers. The initial angular momentum is,

$$h_0 = \begin{bmatrix} 0 \\ 0 \\ -1 \end{bmatrix} \quad (50)$$

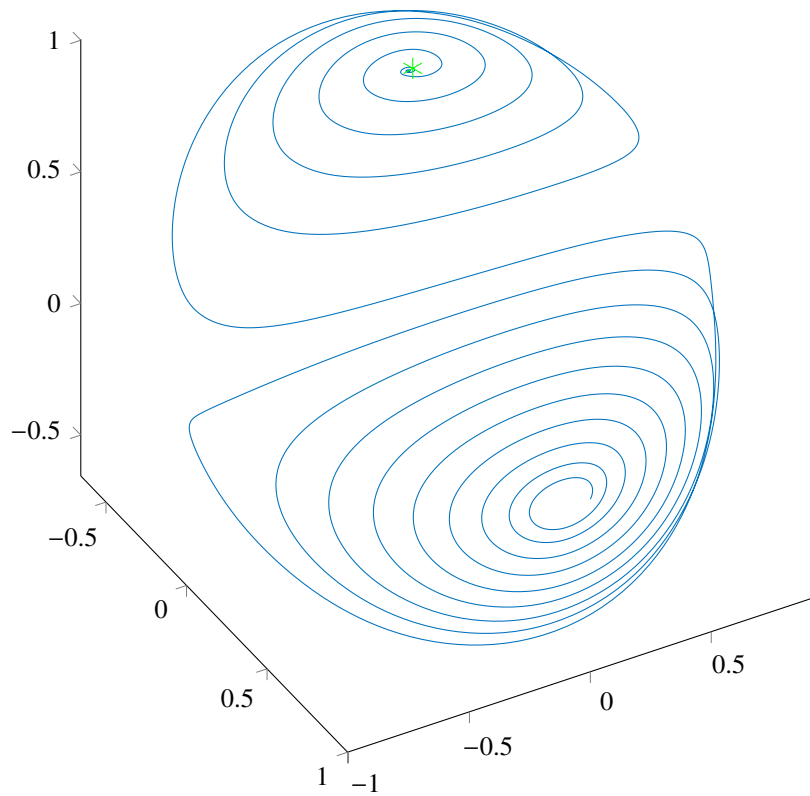


Figure 6. Flat-spin recovery trajectory

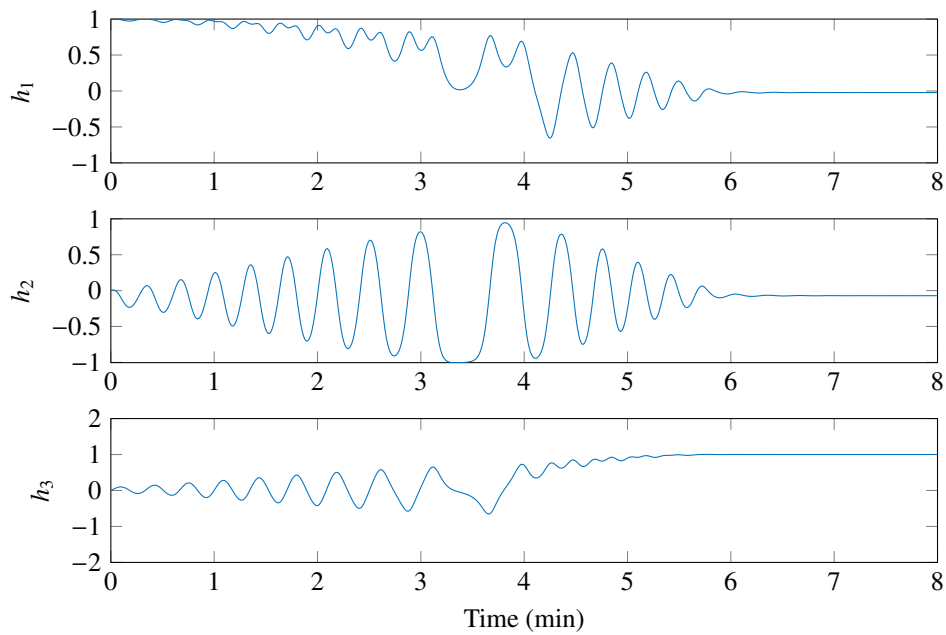


Figure 7. Flat-spin recovery momentum components

and the desired final angular momentum is again set to:

$$h_d = \begin{bmatrix} 0 \\ 0 \\ 1 \end{bmatrix} \quad (51)$$

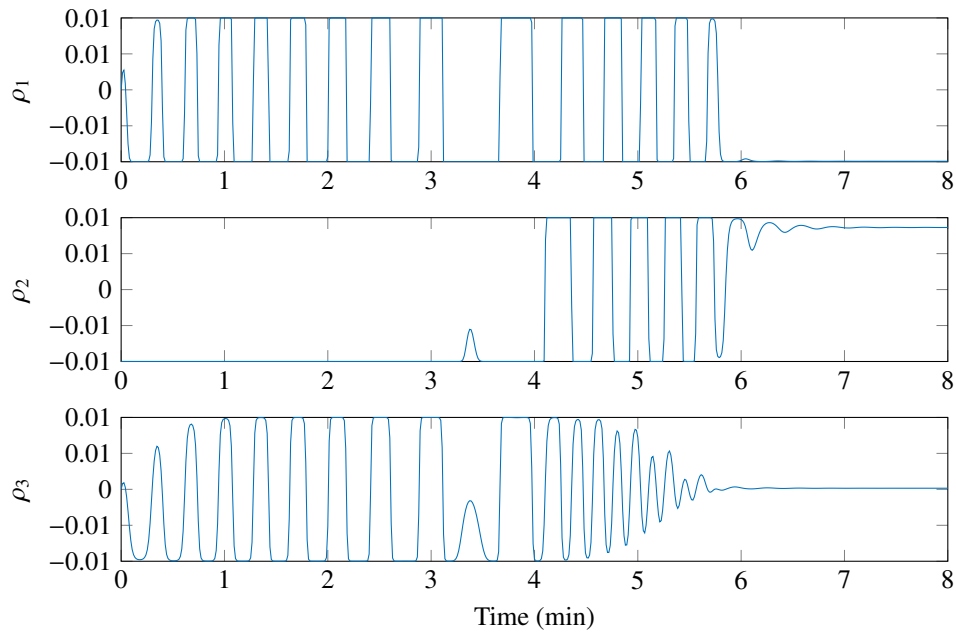


Figure 8. Flat-spin recovery reaction wheel momenta

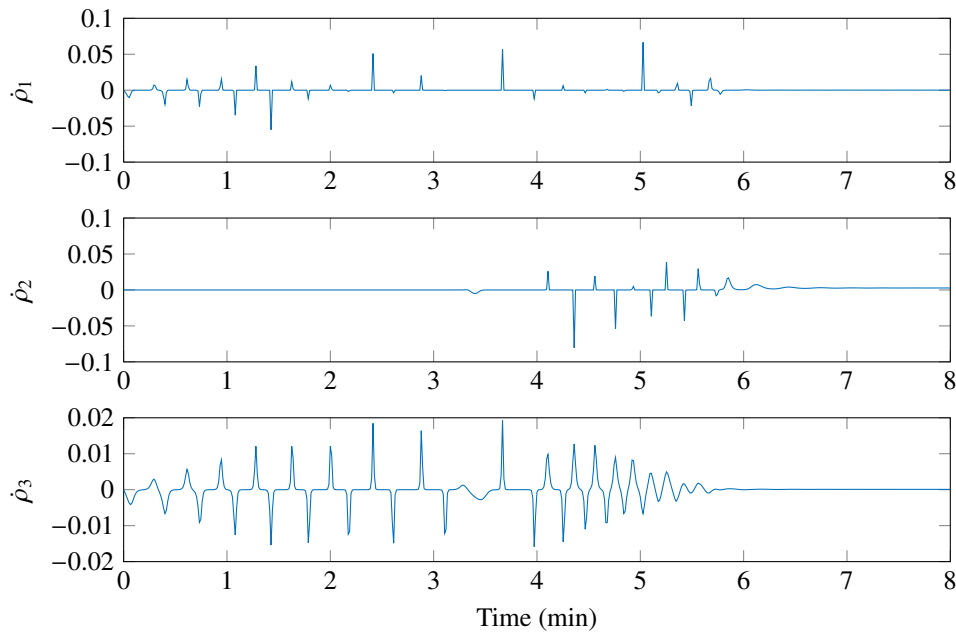


Figure 9. Flat-spin recovery reaction wheel torques

Figure 10 shows the closed-loop trajectory of the system, while figures 11–13 show the system momentum, reaction wheel momentum, and reaction wheel torque components, respectively. Once again, the controller demonstrates rapid convergence. This example also illustrates the behavior of the closed-loop system around the point $-\mathbf{h}_d$. As discussed in section V, noise and modeling errors ensure that the system is perturbed away from this unstable equilibrium.

IX. Conclusions

The control laws developed in this study provide a unified solution for both flat-spin recovery and spin inversion of spin-stabilized spacecraft. They are shown to be almost-globally asymptotically stabilizing using a Lyapunov function

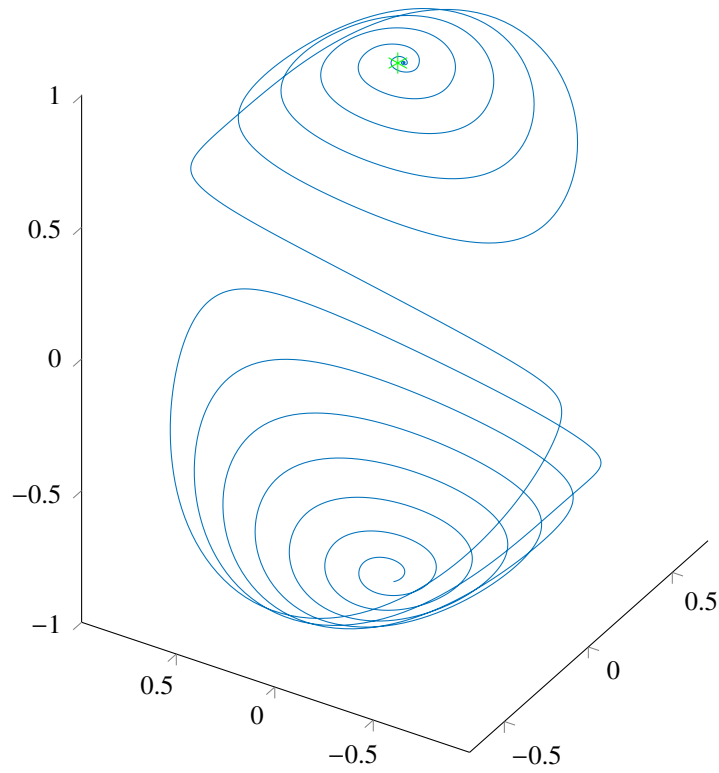


Figure 10. Spin inversion trajectory

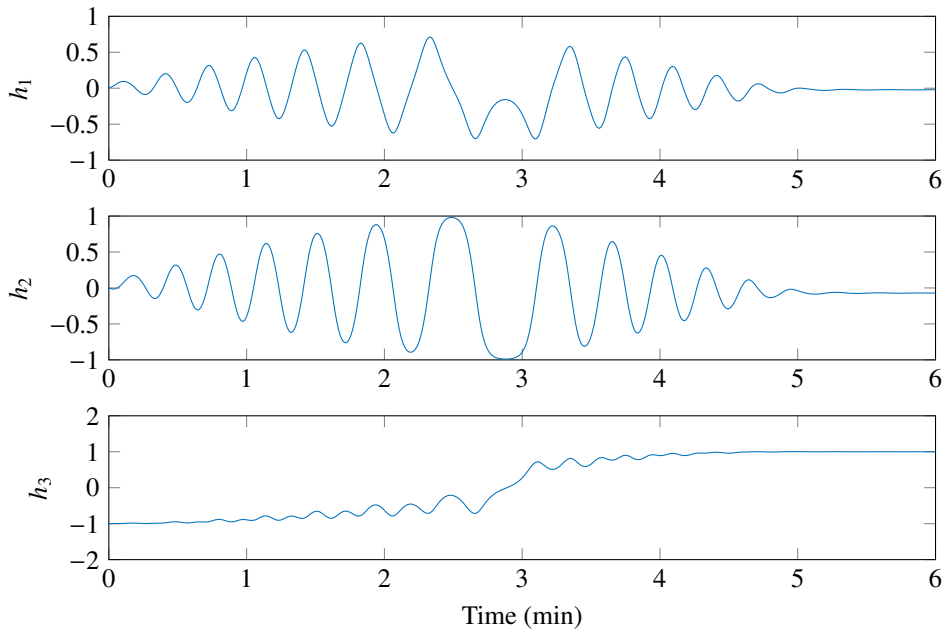


Figure 11. Spin inversion momentum components

argument, and their performance is also demonstrated in the presence of model errors and actuator limits through numerical simulation. Lastly, the controllers have a simple mathematical form and are easy to tune, making them practical for implementation in flight software.

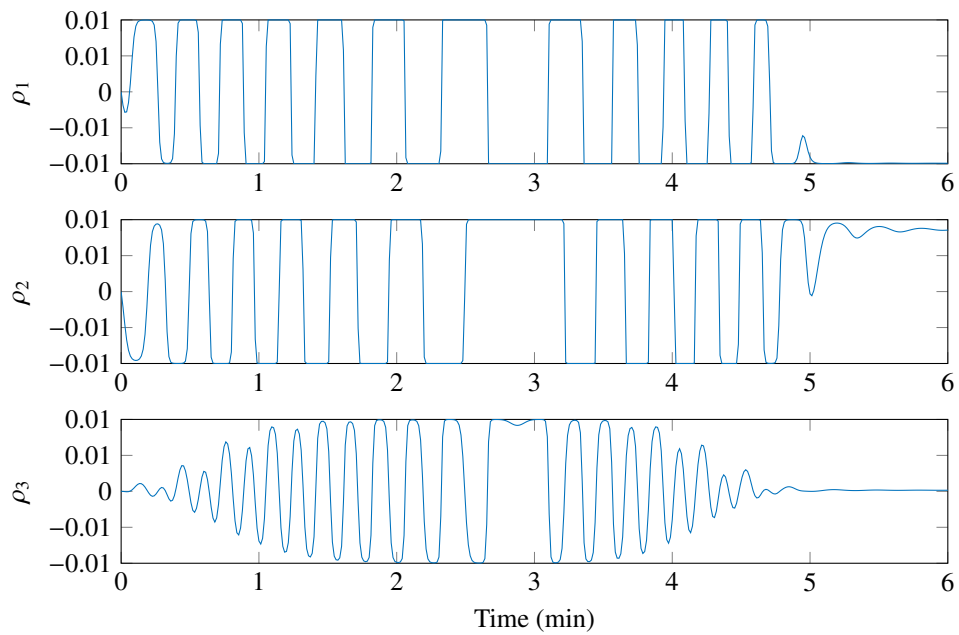


Figure 12. Spin inversion reaction wheel momenta

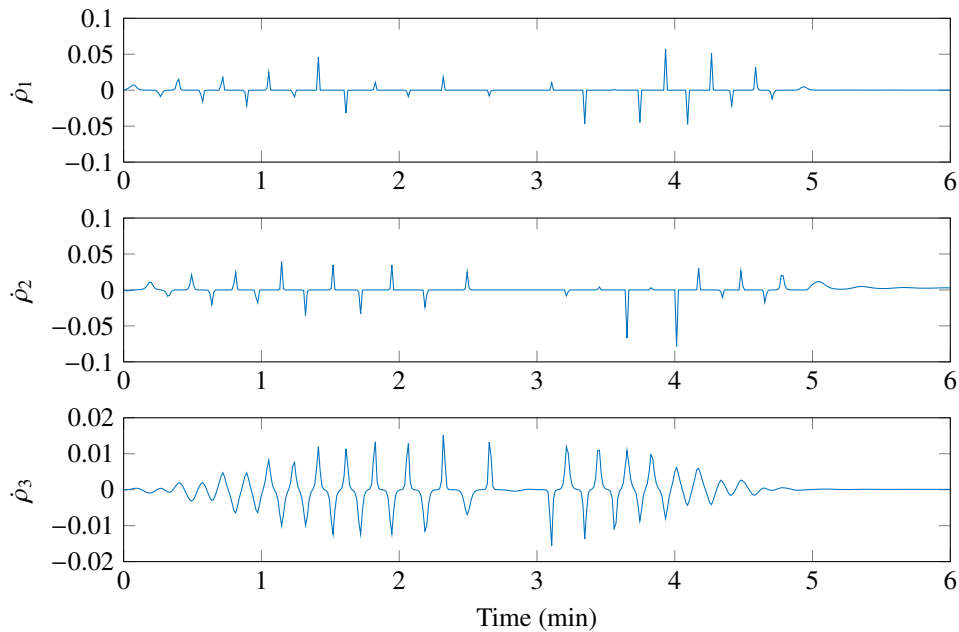


Figure 13. Spin inversion reaction wheel torques

References

- [1] Bracewell, R. N. and Garriott, O. K., “Rotation of Artificial Earth Satellites,” *Nature*, Vol. 182, Sep 1958, pp. 760–762.
- [2] Devey, W. J., Field, C. F., and Flook, L., “An Active Nutation Control System for Spin Stabilized Satellites,” *Automatica*, Vol. 13, 1977, pp. 161–172.
- [3] Fish, C. S., Swenson, C. M., et al., “Design, Development, Implementation, and On-orbit Performance of the Dynamic Ionosphere CubeSat Experiment Mission,” *Space Science Reviews*, Vol. 181, Feb 2014, pp. 61–120.
- [4] Manchester, Z., Peck, M., and Filo, A., “KickSat: A Crowd-Funded Mission to Demonstrate the World’s Smallest Spacecraft,” *AIAA/USU Conference on Small Satellites*, Logan, UT, Aug 2013.

- [5] Wise, E. D., Pong, C. M., et al., "A Dual-Spinning, Three-Axis-Stabilized CubeSat for Earth Observations," *AIAA Guidance, Navigation, and Control Conference*, Boston, Aug 2013.
- [6] Barba, P. M., Furumoto, N., and Leliakov, I. P., "Techniques for Flat-Spin Recovery of Spinning Satellites," *AIAA Guidance and Control Conference*, Key Biscayne, FL, Aug 1973, pp. 859–867.
- [7] Gebman, J. R. and Mingori, D. L., "Perturbation Solution for the Flat Spin Recovery of a Dual-Spin Spacecraft," *AIAA Journal*, Vol. 14, No. 7, 1976, pp. 859–867.
- [8] Lawrence, D. A. and Holden, T. E., "Essentially Global Asymptotically Stable Nutation Control Using a Single Reaction Wheel," *Journal of Guidance, Control, and Dynamics*, Vol. 30, No. 6, 2007, pp. 1783–1793.
- [9] Rahn, C. D. and Barba, P. M., "Reorientation Maneuver for Spinning Spacecraft," *Journal of Guidance, Control, and Dynamics*, Vol. 14, No. 4, Jul 1991, pp. 724–728.
- [10] Beachley, N. H. and Uicker, J. J., "Wobble-spin technique for spacecraft inversion and earth photography," *Journal of Spacecraft and Rockets*, Vol. 6, No. 3, Mar 1969, pp. 245–248.
- [11] Beachley, N. H., "Inversion of Spin-Stabilized Spacecraft by Mass Translation - Some Practical Aspects," *Journal of Spacecraft and Rockets*, Vol. 8, No. 10, Oct 1971, pp. 1078–1080.
- [12] Myung, H.-S. and Bang, H., "Predictive Nutation and Spin Inversion Control of Spin-Stabilized Spacecraft," *Journal of Spacecraft and Rockets*, Vol. 47, No. 6, 2010, pp. 1010–1022.
- [13] Lu, P., "Nonlinear Predictive Controllers for Continuous Systems," *Journal of Guidance, Control, and Dynamics*, Vol. 17, No. 3, 1994, pp. 553–560.
- [14] Khalil, H., *Nonlinear Systems*, Prentice Hall, Englewood Cliffs, NJ, 3rd ed., 2002.
- [15] Slotine, J. and Li, W., *Applied Nonlinear Control*, Prentice Hall, Englewood Cliffs, NJ, 1991.
- [16] Hughes, P., *Spacecraft Attitude Dynamics*, Dover Books on Aeronautical Engineering, Dover Publications, Mineola, New York, 2004.
- [17] Masaitis, C., "On the motion of two linked bodies," *Archive for Rational Mechanics and Analysis*, Vol. 8, No. 1, 1961, pp. 23–35.
- [18] Wittenburg, J., *Dynamics of Systems of Rigid Bodies*, Teubner, Stuttgart, 1st ed., 1977.
- [19] Bhat, S. P. and Bernstein, D. S., "A topological obstruction to continuous global stabilization of rotational motion and the unwinding phenomenon," *Systems and Control Letters*, Vol. 39, No. 1, 2000, pp. 63–70.
- [20] Shampine, L. F. and Reichelt, M. W., "The Matlab ODE Suite," *SIAM Journal on Scientific Computing*, Vol. 18, No. 1, 1997, pp. 1–22.